Dartmouth College

Dartmouth Digital Commons

12-20-2004

Signature of Electron Capture in Iron-rich Ejecta of SN 2003du

Peter Hoflich
University of Texas at Austin

Christopher L. Gerardy
University of Texas at Austin

Ken-ichi Nomoto
University of Tokyo

Kentaro Motohara
University of Tokyo

Robert A. Fesen
Dartmouth College

Follow this and additional works at: https://digitalcommons.dartmouth.edu/facoa

Part of the Stars, Interstellar Medium and the Galaxy Commons

SIGNATURE OF ELECTRON CAPTURE IN IRON-RICH EJECTA OF SN 2003du[1]

PETER HÖFLICH,[2] CHRISTOPHER L. GERARDY,[2,3] KEN'ICHI NOMOTO,[4] KENTARO MOTOHARA,[5]
ROBERT A. FESEN,[6] KEIICHI MAEDA,[7] TAKUYA OHKUBO,[4] AND NOZOMU TOMINAGA[4]
Received 2004 June 24; accepted 2004 September 1

ABSTRACT

Late-time near-infrared and optical spectra of the normal–bright Type Ia supernova 2003du about 300 days after the explosion are presented. At this late epoch, the emission profiles of well-isolated [Fe II] lines (in particular that of the strong 1.644 μm feature) trace out the global kinematic distribution of radioactive material in the expanding supernova ejecta. In SN 2003du, the 1.644 μm [Fe II] line seems to show a flat-topped profile, indicative of a thick but hollow-centered expanding shell, rather than a strongly peaked profile that would be expected from a "center-filled" distribution. Based on detailed models for exploding Chandrasekhar-mass white dwarfs, we show that the feature is consistent with spherical explosion models. Our model predicts a central region of nonradioactive electron capture elements up to 2500–3000 km s^{-1} as a consequence of burning under high density and an extended region of radioactive ^{56}Ni up to 9000–$10,000$ km s^{-1}. Furthermore, our analysis indicates that the 1.644 μm [Fe II] line profile is not consistent with strong mixing between the regions of electron-capture isotopes and the ^{56}Ni layers, as is predicted by detailed three-dimensional models for nuclear deflagration fronts. We discuss the possibility that the flat-topped profile could be produced as a result of an infrared catastrophe and conclude that such an explanation is unlikely. We discuss the limitations of our analysis and place our results into context by comparison with constraints on the distribution of radioactive ^{56}Ni in other SNe Ia and briefly discuss the potential implications of our result for the use of SNe Ia as cosmological standard candles.

Subject headings: nuclear reactions, nucleosynthesis, abundances — supernovae: general —
supernovae: individual (SN 2003du)

Online material: color figures

1. INTRODUCTION

There is general agreement that Type Ia Supernovae (SNe Ia) are the results of thermonuclear explosions of degenerate C/O white dwarfs (WDs), most likely close to the Chandrasekhar limit for the majority of events because these allow a reasonably good reproduction of the optical/infrared light curves (LCs) and spectra of SNe Ia. However, despite the success of Chandrasekhar-mass models, questions remain concerning the detailed physics of the burning front, the ignition process, and the roles of preconditioning and the progenitor of the WD prior to the explosive phase. For recent reviews see Branch (1998), Höflich et al. (2003), and Nomoto et al. (2003).

The distribution of the iron-group elements is key to answer these questions. It has long been recognized that late-time spectra of SNe Ia, dominated by forbidden lines of Fe-peak elements, are an excellent probe of the amount and distribution of radioactive ^{56}Ni (Axelrod 1980a, 1980b; Meyerott 1980). After about day 200, the energy input is dominated by local energy deposition from positrons, and the envelope is almost transparent, allowing for the direct observation of the entire distribution of radioactive matter and making the result rather insensitive to radiation transport effects. However, the total amount of Ni is still rather uncertain because the emission depends sensitively on the redistribution of energy within an ion (see also "IR catastrophe"; Axelrod 1980a; Fransson et al. 1996) and on the ionization mechanism (e.g., Spyromilio et al. 1992; Liu et al. 1997; Bowers et al. 1997).

In principle, line profiles are less sensitive to these effects, since they depend not on the absolute amount of excitation at a certain time but rather on the relative change of the conditions within the envelope. Unfortunately, the spectral features in the optical are produced by a large number of overlapping lines, making the intrinsic emission profiles difficult to untangle. The near-IR contains much more isolated lines, potentially offering the opportunity to look for the remnants of high-velocity plumes in the outer regions of the ^{56}Ni-rich gas and to look for kinematic offsets of the ^{56}Ni distribution from off-center ignition. However, infrared spectroscopic observations at such a late epoch are difficult to obtain and, to date, very late-time (>200 days) IR spectra have only been published for the unusual supernova SN 1991T (Phillips 1993; Spyromilio et al. 1992; Bowers et al. 1997).

Here we present a study of late-time spectra of the "normal–bright" Type Ia SN 2003du, concentrating on NIR spectroscopic observations with the 8.2 m Subaru telescope. In § 2, we discuss the observations and data reduction. In § 3, we describe our models used for the analysis of observations and its implications, which is presented in § 4. In § 5, we discuss the results with an eye toward the broader context. In § 6, we sum up the results and comment on the limits of our study and future perspectives.

2. OBSERVATIONS AND DATA REDUCTION

SN 2003du was discovered in UGC 9391 by the Lick Observatory and Tenegra Observatory Supernova Searches (LOTOSS;

[1] Based on data collected at Subaru Telescope, which is operated by the National Astronomical Observatory of Japan, and at McDonald Observatory of the University of Texas at Austin.
[2] McDonald Observatory, University of Texas at Austin, Austin, TX 78712.
[3] W. J. McDonald Postdoctoral Fellow.
[4] Department of Astronomy, University of Tokyo, Hongo 7-3-1, Bunkyo-ku, Tokyo 113-0033, Japan.
[5] Institute of Astronomy, University of Tokyo, 2-21-1 Osawa, Mitaka, Tokyo, Japan.
[6] Department of Physics and Astronomy, Dartmouth College, 6127 Wilder Laboratory, Hanover, NH 03755.
[7] Department of Earth Science and Astronomy, College of Arts and Sciences, University of Tokyo, Meguro-ku, Tokyo 153-8902, Japan.

Schwartz & Holvorcem 2003) on 2003 April 22 (UT) at about 15.9 mag. It was classified as Type Ia on 2003 April 24 by Kotak et al. (2003), who noticed that it resembled SN 2002bo about 2 weeks before maximum light. Early-epoch optical spectroscopy revealed a high-velocity component of the Ca II infrared triplet feature, similar to that seen in SN 2001el, which may be the signature of interaction with circumstellar material, but otherwise the optical evolution appeared normal (Gerardy et al. 2004).

2.1. *Near-Infrared Spectroscopy*

A near-infrared spectrum (1.1–1.8 μm, $R \approx 400$; Fig. 1) of SN 2003du was obtained on 2004 February 27 (296 days after V_{max}) using the OH-airglow Suppressor (OHS; Iwamuro et al. 2001) and the Cooled Infrared Spectrograph and Camera for OHS (CISCO; Motohara et al. 2002) on the Subaru 8.2 m telescope. The observations consisted of two 2000 s exposures, using a 0″.5 slit, with the object dithered 10″ along the slit between exposures. A second, lower S/N spectrum, totaling 1500 s on-target integration time, was obtained on 2004 April 2, (331 days after V_{max}).

Data reduction was performed using standard IRAF routines (Tody 1986). The two exposures were differenced for first-order sky subtraction, then the "negative" spectrum was inverted, shifted, and combined with the "positive" spectrum. Cosmic rays, hot pixels, and other detector defects were removed using the LA-Cosmic package (van Dokkum 2001). Since the 0″.105 pixels oversample the spectrum, the combined data were boxcar filtered 3×3 before one-dimensional spectra were extracted. During the extraction, a second background subtraction was performed using the average background level from the regions adjacent to the extraction aperture. One-dimensional spectra were wavelength calibrated using the standard OHS/CISCO wavelength mapping,[8] shifted to the measured slit position during the observations. The combined atmospheric and instrumental transmission function was removed from the data by following the target observations with observations of an A2 star (SAO 029603) at similar air mass and matching the observed spectrum of the telluric star with stellar atmosphere models of Kurucz (1994).

The S/N of the resulting spectrum is highly wavelength dependent. The data are completely sky-noise dominated, so the S/N is essentially independent of the signal strength from the supernova but is instead strongly dependent on the level of the night-sky emission at a given wavelength. Where strong night-sky emission remains after passing through the OH-suppressor, a narrow region of low S/N is created. This effect can be seen very clearly in the two-dimensional preextraction image shown in Figure 1, in which the bright O_2 band near 1.3 μm is not suppressed by the OHS and creates a band of very low S/N in the resulting data.

The reduced NIR spectrum of SN 2003du on February 27 is shown in Figure 1, with the wavelengths presented in the rest frame of the host galaxy ($cz = 1914$ km s^{-1}; Schneider et al. 1992). The spectrum exhibits broad emission from the [Fe II] 1.257 μm ($a^6D_{9/2}$–$a^4D_{7/2}$) and 1.644 μm ($a^4F_{9/2}$–$a^4D_{7/2}$) lines, which typically dominate nebular Fe spectra in the near-IR (e.g., Nussbaumer & Storey 1980; Oliva et al. 1989, 1990). Surprisingly, the 1.644 μm line appears to show a flat-topped line profile suggestive of an extended envelope with a central hole in the emissivity. In contrast, a filled envelope would produce

[8] For details, refer to the Subaru OHS/CISCO Web site at http://www.naoj.org/Observing/Instruments/OHS/index.html.
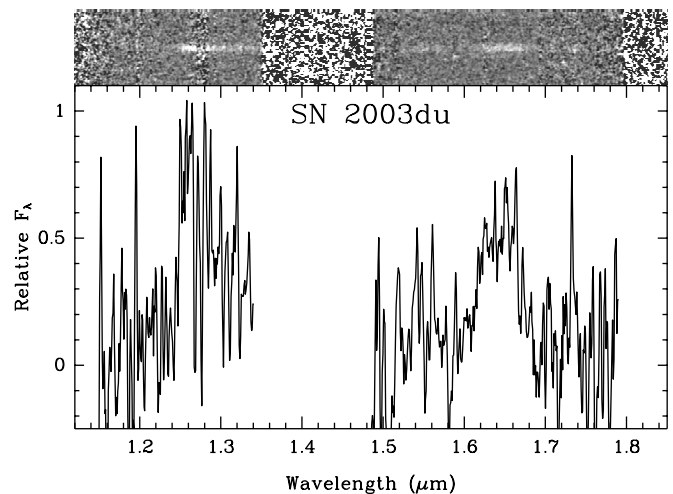

Fig. 1.—NIR spectrum of SN 2003du on 2004 February 27, obtained at the Subaru telescope with the OH-suppressor spectrograph (OHS). The two-dimensional data are shown after the data have been pair-subtracted and stacked but prior to extraction and correction for instrumental response. Note that the S/N is highly wavelength dependent because of the influence of night-sky emission features even with the OH-suppressor.

a strongly peaked line profile. The S/N of the 1.257 μm feature is too low to make any strong statements about the shape of the line profile, but it appears to be consistent with the boxy shape of the 1.644 μm feature. Similarly, the low-S/N spectrum on April 2 is consistent with no significant evolution from the spectrum from February 27. Understanding the nature and implications of this apparent flat-topped emission profile is the subject of our analysis.

2.2. *Optical Spectroscopy*

In addition to the NIR observations, optical spectra (4200–8000 Å, $R \approx 450$) of SN 2003du were obtained on 2004 March 25 (323 days after V_{max}), using the Imaging Grism Instrument on the 2.7 m Harlan J. Smith Telescope at McDonald Observatory. Observations of SN 2003du consisted of four 3600 s exposures using a 2″ east–west oriented slit. Wavelength calibration was achieved by observing Cd, Ar, and Ne arc lamps, and the spectra were flux calibrated using the Massey et al. (1988) standards G191-B2B, Hilt 600, Feige 34, and PG 0823+546.

The reduced optical spectrum is shown in Figure 2. The spectrum is typical of late-time optical spectra of SNe Ia (e.g., Bowers et al. 1997), showing a strong blend of forbidden lines from Fe-peak elements in the 4000–5000 Å region. The feature near 7300 Å is the comparatively isolated [Fe II] 7155 Å line, blended with [Ca II] 7291 and 7324 Å emission and other weak [Fe II] lines at 7142, 7438, and 7648 Å.

3. MODEL CONSTRUCTION

Our quantitative comparison is based on the delayed-detonation model 5p0z22.23, which reproduces the light curve and spectra of a normal–bright SN Ia like SN 2003du reasonably well (Höflich et al. 2002; Gerardy et al. 2004). In delayed-detonation (DD) models, the white dwarf progenitor undergoes supersonic detonation after a period of preexpansion, perhaps because of a phase of subsonic deflagration (Khokhlov 1991; Yamaoka et al. 1992; Woosley & Weaver 1994). We choose a delayed detonation model because this class of model has been found to reproduce the majority of the observed optical/infrared LCs and spectra of SNe Ia reasonably well, including the
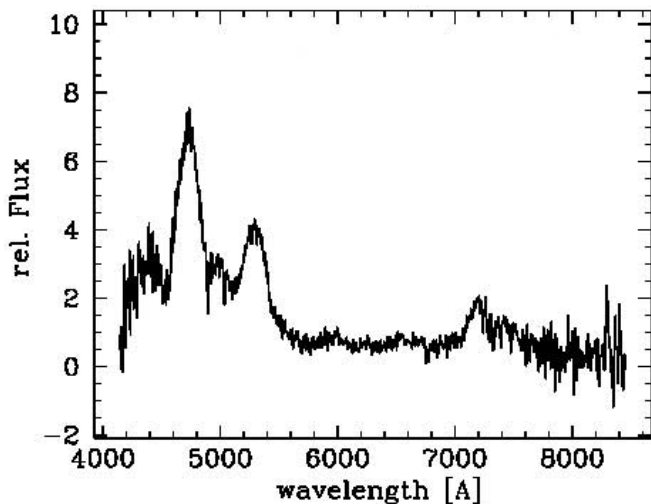
FIG. 2.—Optical spectrum of SN 2003du on 2004 March 27, normalized at 7000 Å.

brightness decline relation (Höflich 1995; Höflich et al. 1996, 2002; Fisher et al. 1995; Höflich & Khokhlov 1996; Wheeler et al. 1998; Lentz et al. 2000). As a reference, we also examine the profile in the context of the well-known deflagration model W7 (Nomoto et al. 1984).

Our results are more generally applicable to all Chandrasekhar-mass models since the structure of the WD, the explosion energy, and the light curves are mainly determined by nuclear physics rather than the details of the nuclear burning ("stellar amnesia"; Höflich et al. 2003). We use these specific models as test beds to interpret the late-time observations.

3.1. *Open Questions of the Explosion Physics*

Despite the successes of delayed detonation models (and W7), questions remain concerning the detailed physics of the burning front (Livne & Arnett 1993; Khokhlov 1995, 2001; Reinecke et al. 1999, 2002; Gamezo et al. 2002), the ignition process, and the role of preconditioning of the WD prior to the explosive phase (Höflich et al. 1998; Lisewski et al. 2000; Höflich & Stein 2002). Overall, the propagation of the detonation front is well understood, but the description of the deflagration front and, in the DD scenario, the mechanism for a deflagration-to-detonation transition (DDT) are persistent unsolved problems, as is the location of the DDT, which, if off-center, may result in off-center distributions of ^{56}Ni.

On a microscopic scale, a deflagration propagates because of heat conduction by electrons. Although the laminar flame speed in SNe Ia is well known, the front has been found to be Rayleigh-Taylor (RT) unstable, increasing the effective speed of the burning front (Nomoto 1982). Current hydrodynamic calculations, starting from central ignitions in static WDs, all show that RT instabilities govern the morphology of the burning front in the regime of linear instabilities, i.e., as long as perturbations remain small. During the first seconds after the runaway, the increase of the flame surface due to RT instabilities remains small, and the effective burning speed is rather small, resulting in the rise of large plumes of burned matter through the WD.

Niemeyer & Woosley (1997) studied the effect of off-center ignition and demonstrated that multiple-spot ignitions will alter the early propagation of the flame. In significantly off-center ignitions, the buildup time of RT instabilities is shorter, corresponding to the larger gravitational acceleration, producing off-center distributions of iron-group elements, although the

overall picture of large, rising plumes still remains unchanged. As a consequence (and in contrast to spherical explosion models), we expect mixing of electron-capture products, formed by high-density burning, with the radioactive ^{56}Ni-rich layers from lower density burning. Note, however, that in all these calculations the constraint of starting from a static WD is not trivial, as the morphology (and, consequently, the effective burning speed) of blobs depends on small-scale motions of the background produced prior to the explosive burning phase (Höflich & Stein 2002), particularly in the earliest burning stage.

Probing the properties of the deflagration burning front directly with observations has proven difficult because the signatures of the deflagration are mostly wiped out during the detonation phase in normal–bright SNe Ia (Livne 1999; Gamezo et al. 2003). This provides the justification for our approach and the explanation for our use of a spherical DD model as baseline.

3.2. *Model Construction*

For this study, the delayed detonation model 5p0z22.23 (Fig. 3) was chosen. We use also the deflagration model W7 as additional reference.

We consider the explosion of a Chandrasekhar-mass white dwarf that originates from a star with a main sequence mass of 5 $M_\odot$ and solar composition. At the time of the explosion, the central density is 2×10^9 g cm^{-3}. The nuclear burning starts as a deflagration with a parameterized description of rate of burning based on three-dimensional models by Khokhlov (2001). When the density reaches $\rho_{tr} = 2.5 \times 10^7$ g cm^{-3}, the detonation is triggered. The final density and chemical structures are given in Figure 3.

The preexpansion of the WD is determined only by the amount of burning during the deflagration phase and not the detailed properties of the deflagration front. In one-dimensional spherical models ρ_{tr} is thus a convenient parameterization of the amount of burning during the deflagration. After the detonation is triggered, the burning products depend mainly on the density under which burning occurs. Because the detonation wave propagates rapidly through the WD at slightly above the sound speed, the outcome is determined primarily by the density structure of the (puffed up) WD at the time of the DDT. As a result, the final density and chemical profiles are rather generic for all DD models.

Our analysis of the line profiles is based on radiation transport models using our Monte Carlo scheme implemented in HYDRA, including detailed γ-ray transport and energy deposition of fast electrons (see Höflich 2003a, 2003b, and references therein). Forbidden lines are included based on Kurucz's database (1993) and Nussbaumer & Storey (1988a, 1988b) and supplemented with line lists given in Liu et al. (1997) and Bowers et al. (1997). Guided by detailed calculations (Ruiz-Lapuente et al. 1995; Liu et al. 1997), we assume that the energy input is given by the energy deposition in form of γ-rays and positrons based on our detailed Monte Carlo calculations and that the distribution of the dominant ion is given by the abundance profile in the envelope, which allows us to investigate line profiles. We do not calculate the ionization structure because its details depend sensitively on the assumptions and the processes. The total amount of Fe II varies and, as a consequence, the absolute fluxes are uncertain. For the Fe II distribution, the main difference between models in literature are related to the central region, which may or may not show Fe II as the dominant ionization stage. Here, we use the observations to constrain the conditions at the center and, thus, have to use our approximation.
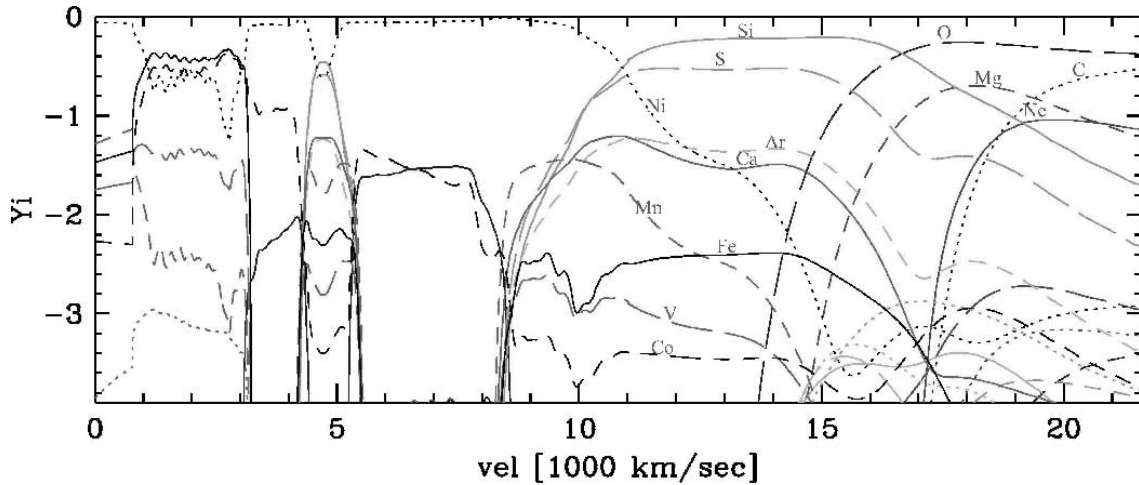
FIG. 3.—Chemical structure of the delayed detonation model. The abundances of stable isotopes and ^{56}Ni are given as a function of the expansion velocity. The curves with the highest abundance close to the center are ^{54}Fe, ^{58}Ni, and ^{56}Fe. The calculation is based on a delayed detonation model with central and transition densities of 2×10^9 g cm^{-3} and 2.5×10^7 g cm^{-3}, respectively. [*See the electronic edition of the Journal for a color version of this figure.*]

Our approach is well supported by the current literature. The most detailed calculations for the ionization structures near day 300 have been published for W7, a model with a chemical structure in the inner regions similar to our delayed detonation model (Ruiz-Lapuente et al. 1995 and Liu et al. 1997, hereafter RL95 and LJS97, respectively). Generally, the results of R95 and LJS97 roughly agree, namely that Fe II is the dominant ionization stage throughout the ^{56}Ni region with little variation in the ionization fraction. Small differences, namely an increase of the Fe III with radius, are present at the outer, high-velocity layers, which contribute to the line wings. However, a significant qualitative difference can be seen close to the center, where R95 find that iron-group elements are mostly neutral and LJS97 find that Fe II dominates Fe I. At an epoch of around 300 days, energy deposition and ionization by γ-rays is of little importance, but collisions with fast electrons are the dominant source of ionization (LJS97). These fast electrons are produced by the energy deposition by positrons that are produced as a consequence of the β^+ decay of ^{56}Co. However, neither LJS97 nor R95 considered the effect of magnetic fields. Whether the fast leptons can leak into the core depends on the physical processes considered and on the magnetic field or, more precisely, on the gyroradius R, which is given by

$$ R = \frac{\sqrt{2 m_e E_e} c}{e B_\perp} \simeq 3.4 \times 10^3 \frac{\sqrt{E_e}}{B_\perp} \text{ cm,} $$

where m_e, E_e, and e are the mass, energy (in MeV), and charge of the fast electron, respectively, and $B_\perp$ is the orthogonal magnetic field. Typical progenitor WD magnetic fields have been estimated to be $\sim 10^5$–10^9 Gauss (Leibundgut 1994). Assuming that the flux is frozen in, the magnetic field evolves as $B_r = B_r(t=0)(r_o/r)^2$. Thus by day 300, the magnetic field is about $\sim 10^{-11}$–10^{-7} Gauss, implying that the gyroradius is about 2% or less of the distance to the inner edge of the ^{56}Ni distribution (see Fig. 3). Even a small $B_\perp$ would keep the electrons local. For comparing the line profiles as a baseline model, we assumed that the local energy input is given by the ^{56}Ni distribution and that the emissivity is given by the abundance distribution.

4. DATA ANALYSIS

4.1. *Delayed Detonation Scenario*

We concentrate on the spectral emission profile of [Fe II] at 1.644 μm, which is essentially unblended at late times. This feature is surrounded by weaker lines from the same multiplet, but in nebular conditions, these lines emit at $\sim 1/3$ or less of the 1.644 μm feature (e.g., Nussbaumer & Storey 1980; Oliva et al. 1989, 1990). As such they may contribute some to the faint wings, but will not affect the bulk of the line profile.

The comparison between the observation on February 27 and the models is given in Figure 4. The flat-topped profile can be well reproduced by the theoretical line profile of our (unmixed) reference model (*thin solid lines*). In this model, the flat top is produced by the lack of radioactive matter (i.e., ^{56}Ni/Co) close the center as a consequence of high-density burning up to an expansion velocity of ~ 3000 km s^{-1}, resulting in nonradioactive electron-capture products (see Fig. 3, and also Brachwitz et al.
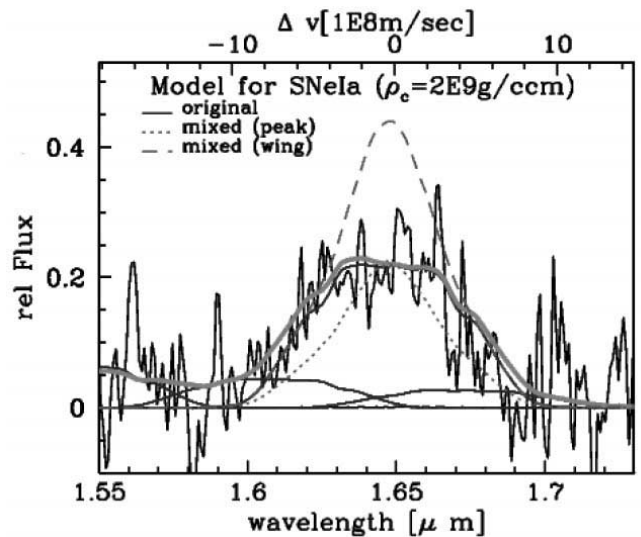

FIG. 4.—NIR spectrum of SN 2003du on 2004 February 27, in comparison with the theoretical line profiles (*thick solid line*). In addition, the individual components of the forbidden [Fe II] transition at 1.644 μm are given for the original delayed detonation model (*thin solid lines*) and mixed chemistry, normalized to the maximum line flux (*dotted line*) and the wings (*dashed line*), respectively. In addition, weaker individual contributions are given for weaker [Fe II] lines (1.599, 1.664, and 1.677 Å). The theoretical spectrum has been shifted by the peculiar velocity of the host galaxy (+1932 km s^{-1}) and a residual velocity of -500 km s^{-1}. [*See the electronic edition of the Journal for a color version of this figure.*]
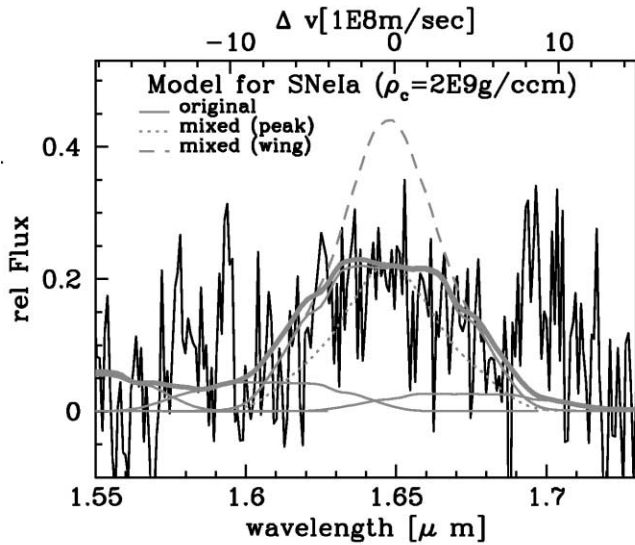
Fig. 5.—NIR spectrum of SN 2003du on 2004 April 2, with 1/3 of the integration time of the spectrum from 27 February. The line is present, and the profile is consistent with little evolution, still seeming to show a flattened profile. However, the S/N of the spectrum is such that it cannot put strong constraints on the shape of the line profile. The comparison line profiles are the same as for Fig. 4. [See the electronic edition of the Journal for a color version of this figure.]
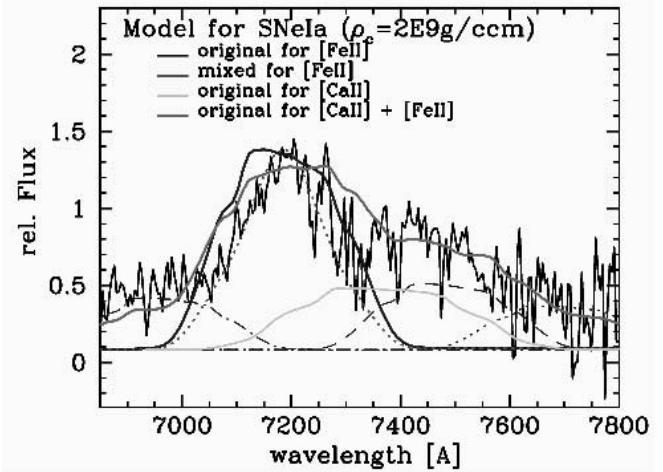

Fig. 6.—Comparison of the observed and theoretical emission profiles (solid, dark gray line) for the region between 6800 and 7790 Å. Fitting the line fluxes, the solid black and light gray lines present fits of the [Fe II] (7155 and 7172 Å) and [Ca II] (7291 and 7324 Å), respectively. Contributions of [Fe II] lines are given for other weaker transitions of [Fe II] (dotted and dash-dotted lines). The dotted line shows the [Fe II] (7155 and 7172 Å) for the mixed model. [See the electronic edition of the Journal for a color version of this figure.]

2000). The extended wings of the feature are produced by the ^{56}Ni/Co region, which extends from ∼3000 km s^{-1} to ∼9000–10,000 km s^{-1}. The slight asymmetry in the theoretical spectrum is caused by optical depth effects due to Thomson, bound-free, and free-free opacities and is consistent with the observed profile, although the S/N is not nearly sufficient to actually detect such a feature. In comparing with the observations, we shifted the model line profile 500 km s^{-1} to the blue. Such a shift might potentially be a signature of an off-center ^{56}Ni distribution, but the shift is too small (≈1 spectral resolution element) to make any significant claim, especially given the S/N of the observed line profile. Because of the shorter integration time of the spectrum obtained on April 2, the level of noise is somewhat higher (Fig. 5). The IR feature at 1.644 μm is still present in this spectrum at roughly the same flux level, and the profile is consistent with that seen in the earlier spectrum.

In light of Rayleigh-Taylor instabilities predicted by three-dimensional deflagration models, the central concentration of electron capture elements in our one-dimensional model might be regarded as somewhat artificial. Three-dimensional deflagration models produce a mixture of radioactive and nonradioactive isotopes within the layers. To simulate this, we also calculated the results from a model with mixing of the inner layers below 8000 km s^{-1}. Similarly, a mixed model will also simulate the effect of penetration of fast electrons into the core in absence of magnetic fields.

In Figure 4, the resulting line profile is shown by the dotted and dashed lines. We show the profile with two normalizations, one normalized to match the observed maximum flux and one adjusted to match the line wings. Although the S/N of the features is low, the observations do not appear to be a good match to either normalization of the mixed profile. The profile matched to the central emission is too narrow, consistently underpredicting the flux in the outer parts of the profile, while the fit to the wings predicts significantly more flux in the center of the line profile than is observed. Since the S/N of the

spectrum is admittedly low, it is difficult to absolutely rule out a more centrally peaked line profile, but the unmixed model certainly seems to be a much better fit to the data. Although the low S/N line profile does not exclude all structures from rising RT plumes, the apparent boxy profile suggests that the rise of such plumes may be significantly limited.

Given implications of the [Fe II] line profile, it is worthwhile to test to see if the profile is present in other spectral features. Unfortunately, the S/N in the 1.257 μm feature is not sufficient to place much of a constraint on the line profile, although it is not inconsistent with the 1.644 μm feature. In the optical spectrum, the features appear more peaked, seemingly in contradiction to the IR feature. However, the features in the 4000–5000 Å are composed of blends of large numbers of forbidden lines from iron-group elements. Thus the profiles of these features are rather weakly linked to the kinematic distribution of radioactive material and, in our model at day 300, do not allow us to analyze its boxiness.[9]

The only relatively clean [Fe II] feature (7155 Å) seems to contradict the observed 1.644 μm profile, showing what seems to be a definite peak at 7200 Å (Fig. 6). Indeed such a profile seems more suggestive of our mixed model (dotted line) than the reference model with the central hole in the ^{56}Ni distribution (black line). However, neither interpretation explains the extended red wing of the observed emission. Instead, both the peaked emission at 7200 Å and the extended red wing extending to about 7550 Å can be well reproduced by two blended flat-topped profiles, consistent with the observed NIR line, produced by [Fe II] 7155 Å and blends of weaker [Fe II] 7438 Å and [Ca II] 7291 and 7324 Å, which have an intrinsic emission ratio of 3 : 2. Note that the relative contribution to the red feature depends on the Ca abundance of the specific model. Some support in favor of a significant Ca II contribution may be taken from the observations because a sufficiently strong Fe feature at 7300 Å would produce a secondary red feature, which has not been observed in SN 2003du (see Fig. 6). The combined blend

---

[9] Note that the profile will change with time, and we did not study the time evolution or a wide range of models.
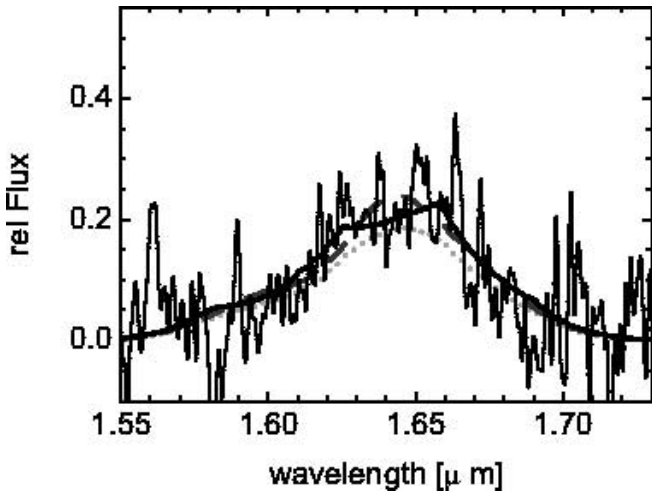
Fɪɢ. 7.—Comparison of the observed [Fe ɪɪ] 1.644 μm feature and a calculated line profile based on the deflagration model, W7, with some variations (Nomoto et al. 1984). We show the results for the original, unmixed model (*dotted line*), with mixing the layers below 8000 km s^{-1} (*dashed line*), and assuming a hole in the emission for layers with velocities less than 3000 km s^{-1} (*solid line*). The fluxes are normalized to the peak of the unmixed model without adjusting the profiles for the other model to the observed data. Thus, a flat-topped profile can be produced by any M_{Ch} model without emission for velocities ≤3000 km s^{-1}. [*See the electronic edition of the Journal for a color version of this figure.*]

explains the red wing of the "plateau" as the edge of the flat-topped [Ca ɪɪ] line and, at the same time, produces the steep red wing and flatter blue wing of the "[Fe ɪɪ]" line through blends. Nevertheless, such ambiguity in the optical demonstrates the need of NIR observations at late time.

4.2. *Deflagration Scenario*

Based on the spherical deflagration model W7, a similar analysis of the data has been carried out by Maeda using the code of Ruiz-Lapuente & Lucy (1992). In Figure 7, we show a comparison of the observed [Fe ɪɪ] 1.644 μm feature and a calculated line profile based on the deflagration model W7, with some variations (Nomoto et al. 1984). We show the results for the original, unmixed model (*dotted line*), with mixing the layers below 8000 km s^{-1} (*dashed line*) and assuming a hole in the emission for layers with velocities less than 3000 km s^{-1} (*solid line*), with the flux normalized to the peak of the unmixed model without adjusting the profiles for the other model to the observed data. At day 300 the resulting profile is not entirely flat topped because of two effects: First, in W7, ^{56}Ni can be found down to about 2200–2300 km s^{-1}, and, second, this calculation still exhibits significant energy deposition by γ-rays near the center. In part, the central γ-ray deposition is caused by the assumption that each scattering process results in full thermalization. Apparently, we require a slightly larger hole of 3000 km s^{-1} to create a sufficiently broad, flat-topped feature.

5. ALTERNATE INTERPRETATIONS

Our suggestion, that the flat-topped profiles of SN 2003du indicate a concentration of electron-capture isotopes in the central region with no or little mixing in of ^{56}Ni, is not the only possible interpretation. For example, in the "infrared catastrophe" picture (Axelrod 1980a), a lack of emission at certain expansion velocities can be caused by a redistribution of energy from the optical/near-IR to the far-IR when the density drops below a certain limit (about 100 days after the

explosion). However, the brightness of SN 2003du is consistent with the predictions from early times rather than showing a rapid drop. Furthermore, the outer, low-density, high-velocity layers should exhibit the effect first, and we see no evolution of the line profiles between 2004 February 27 and April 2. Moreover, the optical spectrum looks typical for late-time spectra. Thus, as none of the other predicted signatures of an IR catastrophe can be identified in the observations, we regard this alternative explanation as unlikely.

A difference in the ionization structure of iron from the one assumed here could be another explanation, since the observed line profile depends on the Fe ɪɪ distribution and, in principle, a shift in the ionization state to either Fe ɪ or Fe ɪɪɪ may produce flat-topped Fe ɪɪ profiles. In principle, a shift to Fe ɪɪɪ may show up in the region around 4700 Å. However, in practice, such analysis is severely hampered by strong blending in this region, which produces very wide features equivalent to ≈20,000 km s^{-1} compared to 3000 km s^{-1} considered here. Deconvolving such a feature from this blend depends sensitively on details of the ionization and excitation structure. In our observations, we do not see evidence for a strong narrow emission component by [Fe ɪɪɪ] in this region although, empirically, some contribution cannot be ruled out.

Detailed calculations for the ionization structures at about day 300 have been published for W7, a model with a chemical structure similar to our delayed detonation model (RL95; LJS97). In these models the ionization balance shifts from Fe ɪɪ to Fe ɪɪɪ from the inner to the outer regions because the recombination rate and charge exchange reactions decrease quadratically with the density in the region with radioactive isotopes. As a consequence, higher ionization stages are seen at larger radii, although the Fe ɪɪ/Fe ɪɪɪ ratio is rather smoothly decreasing with density, without sudden changes in the ionization balance. Thus, the lack of Fe ɪɪ emission from the central layers cannot be attributed to a change in the balance toward Fe ɪɪɪ. Furthermore, in the radioactive region, ionization by (local) positron deposition keeps the Fe ɪɪ/Fe ɪ ratio high. In presence of mixing, we cannot expect a "hole" in the Fe ɪɪ distribution, which leads us back to our basic scenario of a central hole in the ^{56}Ni distribution.

The necessity of a hole of 3000 km s^{-1} in the ^{56}Ni distribution is not unique to these specific models we have examined here. Any M_{Ch} model will require a similar hole to be consistent with the observation. The size of the central region with elements produced by electron capture may, in principle, provide a measure for both the central densities and possible mixing. Currently, however, uncertainties in the treatment of the deflagration front and the electron capture rate do not allow us to discriminate between specific models (Brachwitz et al. 2000).

6. DISCUSSION

6.1. *SN Ia Explosion Physics*

Although the observed profile can be reproduced by spherical models of massive WDs, our results pose a serious challenge to our understanding of the detailed physics of the explosion. All current generation three-dimensional models predict deflagration fronts with properties dominated by slowly growing large-scale Rayleigh-Taylor instabilities that allow the products of high-density nuclear burning to rise in plumes and mix with ^{56}Ni. However, our results suggest that the early phase of the explosion, which leads to the early expansion of the WD, is not dominated by RT instabilities (at least not in the case of SN

2003du), although there were similar suggestions from the analysis of SN 1999by, a very subluminous SNe Ia.

Perhaps the early phases of nuclear burning are dominated by preexisting velocity fields produced prior to the thermonuclear runaway (Höflich & Stein 2002). Alternatively, this phase might be dominated by the rise of a single large bubble of burned material that penetrates the WD surface and triggers a detonation that propagates inward (Plewa et al. 2004). We can speculate that variations in the central density of the WD may be responsible for the appearance of profiles like that apparently seen in SN 2003du or, even more radically, that the preexpansion of the WD prior to the detonation phase is not produced during the explosive phase of burning but rather during the preconditioning phase followed directly by an explosive detonation phase.

6.2. *Comparison With Other SNe Ia*

It is useful to put our findings into context and examine the signatures of mixing the very inner layers in other SNe Ia. As mentioned above, the peculiar SN 1991T is the only other SNe Ia for which late-time (>200 days) NIR line profiles have been published. In contrast to our observations of SN 2003du, the line profiles in SN 1991T were triangular, strongly indicating mixing of the inner layers. Late-time observations of the "normal–bright" SN 1998bu (Meikle 2004; Spyromilio et al. 2004) also seem to show a more centrally peaked profile in the near-IR [Fe II] lines.[10]

Note that in the scenario we suggest here, even in a SN with very little mixing, the flat-topped profile will be a transient phenomenon. At earlier times, the central regions of the ejecta will still be optically thick to γ-rays and will therefore show significant low-velocity emission. As the inner layers become optically thin to γ-rays, the central peak would be expected to fade, leaving a boxy profile like the one discussed here, if the magnetic field in the ejecta is strong enough to prevent the free streaming of fast electrons from the radioactive ejecta into the center region. Eventually the expansion of the ejecta would dilute the magnetic field sufficiently to allow the penetration of fast electrons. The energy deposition would no longer be local, and the central peak would light up again. Thus, this scenario would predict an evolution in which the [Fe II] features start centrally peaked, proceed through a phase of boxy emission, and then return to a peaked emission phase (unless the magnetic field in the WD progenitor is too weak to cause the local trapping of fast electrons, in which case the profile would always remain peaked). Indeed, if such an evolution would be observed in the late-time spectra of a Type Ia SN, the epoch of the second transition to a peaked profile could, in principle, be used to infer the strength of the magnetic field in the central region of the WD progenitor.

The very subluminous SN 1999by presented a different constraint on the kinematics of the ^{56}Ni-rich ejecta. In subluminous SNe Ia, little ^{56}Ni is produced during the detonation, and the Si-rich region extends down to expansion velocities of ≈ 5000 km s^{-1}. As a consequence, the chemical signatures of the deflagration phase will survive the subsequent detonation and has been expected to show up as iron-rich plumes embedded in a Si/S rich region. However, strong mixing can be excluded based on the spectral evolution of SN 1999by at early times (Howell et al. 2001; Höflich et al. 2002).
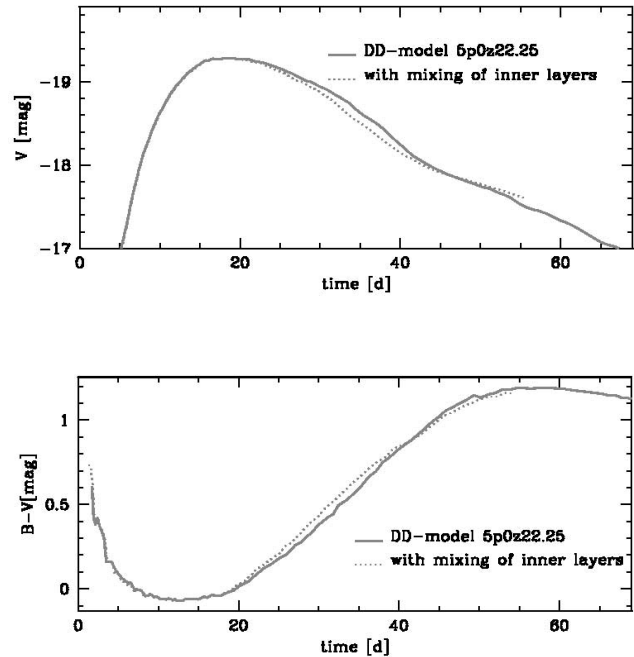

Fig. 8.—Visual light curves and $(B - V)$ for the same delayed detonation model, but with and without mixing of the inner layers (expansion velocities ≤ 8000 km s^{-1}). Our LC calculations take into account detailed hydrodynamics, nuclear networks, radiation transport for low- and high-energy photons, and opacities and include solvers to calculate the atomic level populations (Höflich 2003a, 2003b). [*See the electronic edition of the Journal for a color version of this figure.*]

6.3. *Implications for SN Ia Cosmology*

Our results not only pose a challenge to our present understanding of the physics of the explosion but also raise questions of whether SN 2003du is an exception or the norm and how this will affect our understanding of the diversity of SNe Ia. The implications for the use of supernovae in high-precision cosmology may be significant as it requires a 2% accuracy in distance (Ostriker & Steinhardt 2001; Weller J. & Albrecht 2001). In Figure 8, light curves are shown for two explosion models (Fig. 3) with and without full mixing of layers and with expansion velocities ≤ 8000 km s^{-1} (guided by three-dimensional calculations; Khokhlov 2001), but otherwise identical. Such mixing will bring some ^{56}Ni to the central, high-density region and reduces the ^{56}Ni abundance at other layers. Quantitatively, the results will depend on the details of the mixing, and the differences are of the same order as the numerical accuracy of our calculation. Thus, the LCs are shown here to demonstrate the qualitative effects and the approximate size of the effects.

The difference can be can be understood in terms of energy deposition by the γ-rays and the diffusion time scales of low-energy photons in the SN envelope. The latter strongly decreases with time t (roughly $\propto t^{-2}$; Höflich 1995), and, at maximum light, it is comparable to the expansion time scale. Up until about 2–3 days before maximum light, the luminosity is mostly determined by the outer part of the ^{56}Ni layer, and, consequently, the early light curves are virtually identical. With time, deeper layers start to contribute. Because mixing effectively reduces the ^{56}Ni that contributes to the luminosity prior to about day 30, the LC of the mixed model declines faster and is redder. A competing, opposite effect is related to the energy deposition by γ-rays or, more precisely, the escape probability for high-energy photons. Increasingly, γ-rays produced in the outer layers of the ^{56}Ni

---

[10] However, e.g., the optical spectrum of SN 2003cg around 400 days after maximum light shows a very boxy shape to the [Fe II]/[Ca II] emission feature near 7200 Å (Elias de la Rosa et al. 2004).

distribution can escape and, as a consequence, are lost for heating the envelope. In SNe Ia, the escape probability for γ-rays increases strongly with time from about 10%–15% at maximum light to about 60% at about day 50 (Höflich et al. 1992). Mixing of ^{56}Ni increases the trapping of γ-rays because the inner layers are optically thick. As a consequence, the luminosity of the mixed model is higher and the temperature slightly higher. In conclusion, mixing processes will affect the brightness decline relation and the peak-to-tail ratio on the 0.1 mag level. Depending on the amount of mixing and its dependence on the progenitor, this may cause small but systematic evolutionary effects with redshift.

7. SUMMARY

We have presented late-time near-infrared and optical spectra of the "normal–bright" Type Ia supernova 2003du. We show that late-time infrared spectra provide a probe of the distribution of radioactive ^{56}Ni in the ejecta. The strong, nonblended [Fe II] emission line at 1.644 μm is particularly well suited for such work, and in SN 2003du it appears to exhibit a boxlike profile, whereas the optical [Fe II] features (including the strong, single [Fe II] line near 7200 Å) appear more peaked like those previously seen in other SNe Ia at comparable epochs.

Based on detailed models for exploding Chandrasekhar-mass white dwarfs, we have presented a quantitative analysis of the observations, including optical depth effects (although these are rather small). Using our detonation models, we have shown that the line profile of the 1.644 μm line is consistent with spherical explosion models that produce a central region of electron-capture elements up to $\approx$2500–3000 km s^{-1}, as a consequence of burning under high density, and an extended region of radioactive ^{56}Ni up to $\approx$9000–10,000 km s^{-1}. We have shown that the observed IR line profile is inconsistent with mixing of the region of neutron-rich isotopes with the ^{56}Ni-rich layers. The 1.644 μm line is offset about 500 km s^{-1} relative to the host galaxy, which might indicate a slight shift of the distribution of radioactive elements with respect to the envelope.

The observed peaked profile of the optical [Fe II] feature at 7200 Å and its extended wing can be well reproduced by a blend of [Fe II] 7155 and 7172 Å and weaker lines around 7388 and 7452 Å and [Ca II] 7291/7324 Å, with line profiles consistent with the 1.644 μm feature. Such ambiguity in the interpretation of the optical lines demonstrates the usefulness of NIR observations beyond day 250–300, at phases when γ-ray deposition becomes unimportant for the ionization balance of iron group-elements.

Although a hole in the ^{56}Ni seems to be a necessary condition to produce a flat-topped line profile, we also need to require sufficiently local trapping of fast electrons, as could be produced by weak magnetic fields. Higher signal-to-noise observations of other normal–bright SNe Ia, coupled with detailed ionization models, are certainly needed and will provide insight into the diversity (and causes thereof) in SNe Ia, as well as into possible sources of evolutionary effects at higher redshift.

While the flattened [Fe II] 1.644 μm profile is consistent with our one-dimensional models, it presents a challenge to our understanding of the physics in the earliest phase of the explosion, since all current three-dimensional models of the deflagration phase predict significant mixing in the innermost regions. This result for SN 2003du, while differing significantly from the late-time observations of the unusual SN 1991T, places constraints on the mixing of ^{56}Ni during the deflagration that are similar to constraints placed on the mixing in the extremely subluminous SN 1999by. We now have examples of SNe Ia in which mixing may be suggested (SN 1991T and SN 1998bu), and in which it is excluded, or at least very much limited (SN 1999by and SN 2003du). Understanding these phenomena will have significant implications both for the physics of SN Ia explosions and for their use as cosmological probes.

Finally, we also have to address the limitations of this study, which are subject to ongoing projects. Programs at Subaru will increase the number of SNe Ia with late-time IR observations and study the spectral evolution over time. Detailed calculations are underway for the ionization structure that include magnetic fields with the goal to study their influence on the spectra and spectral evolution.

REFERENCES

Axelrod, T. S. 1980a, in Proc. Texas Workshop on Type I Supernovae, ed. J. C. Wheeler (Austin: Univ. Texas, Austin), 80
———. 1980b, Ph.D. thesis, Univ. California, Santa Cruz
Bowers, E. J. C., Meikle, W. P. S., Geballe, T. R., Walton, N. A., Pinto, P. A., Dhillon, V. S., Howell, S. B., & Harrop-Allin, M. K. 1997, MNRAS, 290, 663
Brachwitz, F., et al. 2000, ApJ, 536, 934
Branch, D. 1998, ARA&A, 36, 17
Elias de la Rosa, N., Turatto, M., Cappellaro, E., Stanishev, V., Kotak, R., & Pignata, G. 2004, in Supernovae as Cosmological Lighthouses, ed. M. Turatto, et al. (San Francisco: ASP), in press
Fisher, A., Branch, D., Höflich, P., & Khokhlov, A. 1995, ApJ, 447, L73
Fransson, C., Lundqvist, P., & Chevalier, R. A. 1996, ApJ, 461, 993
Gamezo, V. N., Khokhlov, A. M., & Oran, E. S. 2002, BAAS, 34, 663
Gamezo, V. N., Khokhlov, A. M., Oran, E. S., Chtchelkanova, A. Y., & Rosenberg, R. O. 2003, Science, 299, 77
Gerardy, C. L., Höflich, P., Fesen, R. A., Marion, G. H., Nomoto, K., Quimby, R., Schaefer, B. E., Wang, L., & Wheeler, J. C. 2004, ApJ, 607, 391

Höflich, P. 1995, ApJ, 443, 89
———. 2003a, in ASP Conf. Ser. 288, Stellar Atmosphere Modeling, ed. I. Hubeny, D. Mihalas, & K. Werner (San Francisco: ASP), 185
———. 2003b, in ASP Conf. Ser. 288, Stellar Atmosphere Modeling, ed. I. Hubeny, D. Mihalas, & K. Werner (San Francisco: ASP), 371
Höflich, P., Gerardy, C., Fesen, R., & Sakai, S. 2002, ApJ, 568, 791
Höflich, P., Gerardy, C., Linder, E., & Marion, H. 2003, in Stellar Candles for the Extragalactic Distance Scale, ed. D. Alloin & W. Gieren (Berlin: Springer), 203
Höflich, P., & Khokhlov, A. 1996, ApJ, 457, 500
Höflich, P., Khokhlov, A., Wheeler, J. C., Phillips, M. M., Suntzeff, N. B., & Hamuy, M. 1996, ApJ, 472, L81
Höflich, P., & Stein, J. 2002, ApJ, 568, 779
Höflich, P., Wheeler, J. C., & Thielemann, F. K. 1998, ApJ, 495, 617
Höflich, P., Khokhlov, A., & Müller, E. 1992, A&A, 259, 549
Howell, A., Höflich, P., Wang, L., & Wheeler, J. C. 2001, ApJ, 556, 302
Iwamuro, F., Motohara, K., Maihara, T., Hata, R., & Harashima, T. 2001, PASJ, 53, 355

Khokhlov, A. M. 1991, A&A, 245, 114
———. 1995, ApJ, 449, 695
———. 2001, preprint (astro-ph/0008463)
Kotak, R., Meikle, W. P. S., & Rodriguez-Gil, P. 2003, IAU Circ., 8122, 3
Kurucz, R. L. 1993, Kurucz CD-ROM 1, Atomic Data for Opacity Calculations (Cambridge: SAO)
———. 1994, Kurucz CD-ROM 19, Solar Abundance Model Atmospheres for 0, 1, 2, 4, 8 km/s (Cambridge: SAO)
Leibundgut B. 1994, Proc. 34th Herstmonceux Conf., Circumstellar Media in the Late Stages of Stellar Evolution, ed. R. E. S. Clegg, I. R. Stevens, & W. P. S. Meikle (Cambridge: Cambridge Univ. Press), 100
Lentz, E. J., Baron, E., Branch, D., Hauschildt, P., & Nugent, P. E. 2000, ApJ, 530, 966
Lisewski, A. M., Hillebrandt, W., Woosley, S. E., Niemeyer, J. C., & Kerstein, A. R. 2000, ApJ, 537, 405
Liu, W., Jeffery, D. J., & Schultz, D. R. 1997, ApJ, 483, L107 (LJS97)
Livne, E. 1999, ApJ, 527, L97
Livne, E., & Arnett, D. 1993, ApJ, 415, L107
Massey, P., Strobel, K., Barnes, J. V., & Anderson, E. 1988, ApJ, 328, 315
Meikle, P. 2004, in Supernovae as Cosmological Lighthouses, ed. M. Turatto, et al. (San Francisco: ASP), in press
Meyerott, R. E. 1980, ApJ, 239, 257
Motohara, K., et al. 2002, PASJ, 54, 315
Niemeyer, J. C., & Woosley, S. E. 1997, ApJ, 475, 740
Nomoto, K. 1982, ApJ, 253, 798
Nomoto, K., Thielemann, F.-K., & Yokoi, K. 1984, ApJ, 286, 644
Nomoto, K., Uenishi, T., Kobayashi, C., Umeda, H., Ohkubo, T., Hachisu, I., & Kato, M. 2003, in From Twilight to Highlight: The Physics of Supernovae, ed. W. Hillebrandt & B. Leibundgut (Berlin: Springer), 115

Nussbaumer, H., & Storey, P. J. 1980, A&A, 89, 308
———. 1988a, A&A, 193, 327
———. 1988b, A&A, 200, L25
Oliva, E., Moorwood, A. F. M., & Danziger, I. J. 1989, A&A, 214, 307
———. 1990, A&A, 240, 453
Ostriker, P., & Steinhardt, P. J. 2001, Sci. Am., 284, 47
Phillips, M. M. 1993, ApJ, 413, L105
Plewa, T., Calder, A. C., & Lamb, D. Q. 2004, ApJ, 612, L37
Reinecke, M., Hillebrandt, W., & Niemeyer, J. C. 1999, A&A, 347, 739
———. 2002, A&A, 391, 1167
Ruiz-Lapuente, P., Kirshner, R. P., Phillips, M. M., Challis, P. M., Schmidt, B. P., Filippenko, A. V., & Wheeler, J. C. 1995, ApJ, 439, 60 (RL95)
Ruiz-Lapuente, P., & Lucy, L. 1992, ApJ, 400, 127
Schneider, S. E., Thuan, T. X., Magnum, J. G., & Miller, J. 1992, ApJS, 81, 5
Schwartz, M., & Holvorcem, P. R. 2003, IAU Circ., 8121, 2
Spyromilio, J., Meikle, W. P. S., Allen, D. A., & Graham, J. R. 1992, MNRAS, 258, 53P
Spyromilio, J., Gilmozzi, R., Sollerman, J., Leibundgut, B., Fransson, C., & Cuby, J.-C. 2004, A&A, 426, 547
Tody, D. 1986, Proc. SPIE, 627, 733
van Dokkum, P. G. 2001, PASP, 113, 1420
Weller J., & Albrecht, A. 2001, Phys. Rev. Lett., 86, 1939
Wheeler, J. C., Höflich, P., Harkness, R. P., & Spyromilio, J. 1998, ApJ, 496, 908
Woosley, S. E., & Weaver, T. A. 1994, ApJ, 423, 371
Yamaoka, H., Nomoto, K., Shigeyama, T., & Thielemann, F. 1992, ApJ, 393, L55